THE JOURNAL OF BIOLOGICAL CHEMISTRY VOL. 286, NO. 45, pp. 39188–39199, November 11, 2011

Fibronectin Aggregation and Assembly

THE UNFOLDING OF THE SECOND FIBRONECTIN TYPE III DOMAIN[*S]

Received for publication, May 18, 2011, and in revised form, September 12, 2011 Published, JBC Papers in Press, September 23, 2011, DOI 10.1074/jbc.M111.262337

Tomoo Ohashi[1] **and Harold P. Erickson**

From the Department of Cell Biology, Duke University Medical Center, Durham, North Carolina 27710

The mechanism of fibronectin (FN) assembly and the self-association sites are still unclear and contradictory, although the N-terminal 70-kDa region (^{I}1–9) is commonly accepted as one of the assembly sites. We previously found that ^{I}1–9 binds to superfibronectin, which is an artificial FN aggregate induced by anastellin. In the present study, we found that ^{I}1–9 bound to the aggregate formed by anastellin and a small FN fragment, ^{III}1–2. An engineered disulfide bond in ^{III}2, which stabilizes folding, inhibited aggregation, but a disulfide bond in ^{III}1 did not. A gelatin precipitation assay showed that ^{I}1–9 did not interact with anastellin, ^{III}1, ^{III}2, ^{III}1–2, or several ^{III}1–2 mutants including ^{III}1–2KADA. (In contrast to previous studies, we found that the ^{III}1–2KADA mutant was identical in conformation to wild-type ^{III}1–2.) Because ^{I}1–9 only bound to the aggregate and the unfolding of ^{III}2 played a role in aggregation, we generated a ^{III}2 domain that was destabilized by deletion of the G strand. This mutant bound ^{I}1–9 as shown by the gelatin precipitation assay and fluorescence resonance energy transfer analysis, and it inhibited FN matrix assembly when added to cell culture. Next, we introduced disulfide mutations into full-length FN. Three disulfide locks in ^{III}2, ^{III}3, and ^{III}11 were required to dramatically reduce anastellin-induced aggregation. When we tested the disulfide mutants in cell culture, only the disulfide bond in ^{III}2 reduced the FN matrix. These results suggest that the unfolding of ^{III}2 is one of the key factors for FN aggregation and assembly.

Fibronectin (FN)[2] is a secreted protein expressed in the liver and circulated in blood as a soluble dimer (1). In addition to this plasma FN, some cell types, such as fibroblasts and endothelial cells, secrete FN and assemble it into extracellular matrix fibrils. FN is a modular protein containing 12 FN type I (FNI) domains, two FN type II domains, and 15–17 FN type III (FNIII) domains (2, 3). Two cysteines at the C terminus asymmetrically form interchain disulfide bonds (4, 5). Dimeric FN molecules interact with each other on the cell surface to form matrix fibrils. This process requires cell surface integrins (6–9). Live cell imaging showed that integrin translocation by the actin cytoskeleton is crucial for the early stages of FN matrix assembly (10, 11). More recently, it has been reported that cell-to-cell adhesion via cadherin controls tissue tension and affects FN matrix formation during embryogenesis (12).

The FN matrix had long been thought to be formed by disulfide-bonded FN multimers because the protein migrated at the top of an SDS gel under nonreducing conditions (13–16). However, studies by Chen and Mosher (17) and by our laboratory (18) demonstrated that the FN matrix was composed of FN dimers that are further cross-linked by noncovalent bonds, whose nature is not known. For the past three decades, FN matrix assembly has been studied with FN fragments, antibodies, and deletion mutants. These studies indicate that several domains are crucial for FN matrix formation: ^{I}1–9 (19–24), ^{III}1 and/or ^{III}2 (20, 25, 26), ^{III}4–5 (27), ^{III}7–10 (20, 23, 24), ^{III}12–14 (28), the variable domain (8), ^{I}10–12 (29), and the interchain disulfide bonds at the C terminus involved in dimerization (20). ^{III}7–10 and the variable domain seem to play roles as integrin binding sites. ^{III}4–5, ^{III}12–14, and ^{I}10–12 have contradictory reports (24, 26, 30), so they may only be required for particular cell types or under some conditions. On the other hand, many studies consistently show that ^{I}1–9 is crucial for FN matrix assembly. More precisely, ^{I}1–5 appears to be important because an antibody against this region inhibited FN matrix assembly (23), and mutants in which this region was deleted did not form the FN matrix (20).

In addition to ^{I}1–9, many studies indicate that ^{III}1 and/or ^{III}2 are important for FN matrix assembly. An antibody that recognized ^{III}1 was able to inhibit FN matrix formation (25). Solid phase binding assays showed that ^{III}1–2 and ^{III}2 (without the linker between ^{III}1 and ^{III}2), when adsorbed to plastic, interacted with full-length FN and ^{I}1–9 (26, 31). Sechler *et al.* (26) showed that FN deletion mutants lacking ^{III}2 had significantly decreased matrix assembly.

A recent NMR study showed a unique structure for the domain pair ^{III}1–2 (32). It had been recognized from sequence analysis that there is an 18-amino acid linker between these domains. The NMR structure showed that the A strand of ^{III}2 was disordered, giving a total length of ~35 amino acids for the linker, and further indicated that ^{III}1 and ^{III}2 formed a closed compact structure, with a potential salt bridge between Lys-669 in ^{III}1 and Asp-767 in ^{III}2. These two amino acids were mutated to alanine, giving the mutant designated KADA. The native ^{III}1–2 was found not to bind ^{I}1–5, but the KADA mutation was reported to dramatically enhance binding of ^{I}1–5, as measured by surface plasmon resonance. The authors proposed that

* This work was supported, in whole or in part, by National Institutes of Health Grant CA047056.

[S] The on-line version of this article (available at http://www.jbc.org) contains supplemental Figs. S1–S7.

[1] To whom correspondence should be addressed: Dept. of Cell Biology, Box 3709, Duke University Medical Center, Durham, NC 27710. Tel.: 919-684-6385; Fax: 919-684-8090; E-mail: t.ohashi@cellbio.duke.edu.

[2] The abbreviations used are: FN, fibronectin; superFN, superfibronectin; FNI, fibronectin type I; FNIII, fibronectin type III; FP, fluorescent protein; ANS, 8-anilino-1-naphthalene sulfonate; YPet, yellow fluorescent protein variant; FNBP, fibronectin-binding protein; YFP, yellow fluorescent protein; CFP, cyan fluorescent protein; MBP, maltose-binding protein; FUD, functional upstream domain.

$^{III}1–2$ had a cryptic high affinity binding site for $^{I}1–5$, which could be exposed when the KADA mutations disrupted the binding of $^{III}1$ to $^{III}2$.

Another study used fluorescent protein (FP)-based FRET to explore the conformation of $^{III}1–2$ (33). It was reported elsewhere that a construct with two FNIII domains ($^{III}7–8$) inserted between YFP and CFP showed a negligible FRET signal (34). In contrast, when $^{III}1–2$ was inserted between the FPs, there was a significant FRET signal, consistent with the model that the two domains folded back over the flexible linker and made contact, bringing the N and C termini close together (33). Surprisingly, however, in that study the KADA mutations increased the FRET signal rather than decreasing it. The addition of $^{I}1–9$ reduced the FRET signal of the KADA mutant and had no effect on the FRET of wild type. These authors also suggested a cryptic binding site for $^{I}1–9$ in $^{III}1–2$, which was exposed in the KADA mutant.

In contrast to many protein polymers, which can self-assemble *in vitro*, FN matrix cannot be reconstructed in a test tube. However, there are several approaches to make artificial FN aggregates that resemble the matrix. One of the methods uses anastellin, a truncated form of the first FNIII domain, lacking the A and B β strands (35, 36). Anastellin binds FN to form a large aggregate, called superFN, which has FN matrix-like fibrillar structures when observed by light microscopy. Our previous studies indicated that the opening or unfolding of FNIII domains is important for anastellin binding and aggregation (24, 37). We also found that the N-terminal FN fragment, $^{I}1–9$, which prevented FN matrix formation in cell culture, did not inhibit superFN aggregation. Instead, $^{I}1–9$ co-precipitated with the aggregate (24). In the present study, we further investigated the mechanism of superFN aggregation and FN matrix assembly, by introducing disulfide bonds that prevented opening of the targeted FNIII domains.

EXPERIMENTAL PROCEDURES

Bacterial Protein Expression—The cDNA fragments of $^{III}1–2$, $^{III}1–2$(4aa) (which has a four-amino acid extension at the C terminus), $^{III}1–2\Delta L$ (a 14-amino acid deletion in the linker), $^{III}2$, $L^{III}2$ (with the linker), $^{III}2\Delta A$ (the A strand deletion), and $^{III}2\Delta G$ (the G strand deletion) were amplified by PCR using $^{III}1–5$ (24) as a template and were cloned into the pET15b expression vector (Novagen), which added an N-terminal His tag. The additional N-terminal sequence is MGSSHHHH-HHSSGLVPRGSHM. Fragments $^{III}1$ (SGPV . . . FTTT), $^{III}1–2$ (SGPV . . . SQTT), $^{III}1–2$(4aa) (SGPV . . . SQTTAPDA), $^{III}1–2\Delta L$ (SGPV . . . SQTT without PVTSNTVTGETTPF), $L^{III}2$ (TTST . . . APDA), $^{III}2$ (SPLV . . . SQTT), $^{III}2\Delta A$ (TASS . . . SQTT), $^{III}2\Delta G$ (SPLV . . . GEQS), and $^{III}11$ (EIDK . . . TAVT) were expressed in *Escherichia coli* BL21 (DE3) at 37 °C and were purified with a cobalt column (TALON; Clontech) using standard procedures. Proteins were eluted with imidazole from the column and were dialyzed against 20 mM Tris with 150 mM NaCl (TBS, pH 8.0) or PBS (pH 7.2). Most of the proteins were obtained from the soluble portion of the bacterial lysate except for $^{III}2\Delta G$, which required denaturation and renaturation, using the procedure we reported previously for anastellin (24). Previously generated $^{III}1L$ and anastellin were also used in this study (24). Disulfide mutations in $^{III}1SS$ (S625C and K669C), $^{III}2SS$ (S735C and P778C), and $^{III}11SS$ (S1648C and E1691C) were generated by site-directed mutagenesis with *Pfu* Turbo DNA polymerase (Stratagene), like $^{III}3SS$ engineered previously (37). These cysteines are in equivalent positions in each of the domains as shown in Fig. 1. We also created $^{III}1–2KADA$ (K669A and D767A), $^{III}1SS-2$, and $^{III}1–2SS$ mutants by mutagenesis. The KADA mutations were verified by MALDI-TOF mass spectrometry in addition to DNA sequencing. The amino acid numbering used here follows that of recent publications (32, 33), in which the N-terminal 31-amino acid pre (signal)-pro (furin-recognition) sequence is included. In addition to the FN fragments, we made the functional upstream domain (FUD; from *Streptococcus pyogenes*) construct. The original FUD construct (38) was kindly provided by Drs. Bianca Tomasini-Johansson and Deane Mosher at the University of Wisconsin. Because FUD is a small peptide of 49 amino acids, even with a His tag it was difficult to see in SDS-PAGE at low concentrations. Therefore, we fused FUD to maltose-binding protein (MBP) for visualization. The cDNA fragment of FUD was amplified by PCR using the original construct as a template and was cloned into the author-made MBP expression vector, in which MBP was inserted into the pET24b vector (Novagen). The sequence of the MBP construct is MKIE . . . (MBP) . . . ITKaaaLEHHHHHH (the MBP sequence is underlined). The sequence of the MBP-FUD construct is MKIE . . . (MBP) . . . ITKaaaKDQS . . . (FUD) . . . TEDTaaaLEHHHHHH. These constructs were expressed and purified with standard procedures the same as most of the FN fragments mentioned above. The concentrations of purified proteins were determined from their absorbance at 280 nm using the extinction coefficient of each protein calculated by the Protean computer program (DNAstar Inc.). 5,5′-Dithio-bis (2-nitrobenzoic acid) was used to confirm disulfide bond formation under denaturing conditions (37, 39). SDS-PAGE was performed with standard procedures.

We also created FP-based FRET constructs in which PCR-amplified $^{III}1–2$, $^{III}1–2KADA$, $^{III}2$ and $^{III}2\Delta G$ were cloned into the SpeI and KpnI sites between mYPet and mECFP*. Each FP has a monomeric mutation, A206K (34). The sequence of the FRET construct is MGSSHHHHHHSSGLVPRGSHMggrMVSK . . . (mYPet) . . . ELYKts($^{III}1–2$, $^{III}1–2KADA$, $^{III}2$, or $^{III}2\Delta G$)gtMVSK . . . (mECFP*) . . . ELYKggr (the mYPet and mECFP* sequences are underlined). These FRET constructs were expressed in *E. coli* C41 (DE3) at room temperature and purified as described above. The concentrations of the FRET constructs were estimated from the absorbance at 433 nm using the extinction coefficient of mECFP* (23,500 M^{-1} cm^{-1}).

Mammalian Cell Protein Expression—For transient mammalian cell expression, the cDNA fragments of $^{I}1–9$ (QAQQ . . . TTSS) and $^{I}1–5$ (QAQQ . . . YPSS) were amplified by PCR with FN-YPet/Neo (18) as a template and were cloned into the pHLSec2 vector, which was slightly modified from the original pHLSec vector (40) by Dan Leahy (Johns Hopkins University). This vector has an engineered signal sequence, which gives an additional three amino acids (EGS) at the N terminus of the secreted protein and also adds a C-terminal His tag (EFHHH-HHHHH). FN-YPet (QAQQ . . . DSRE, where monomeric YPet

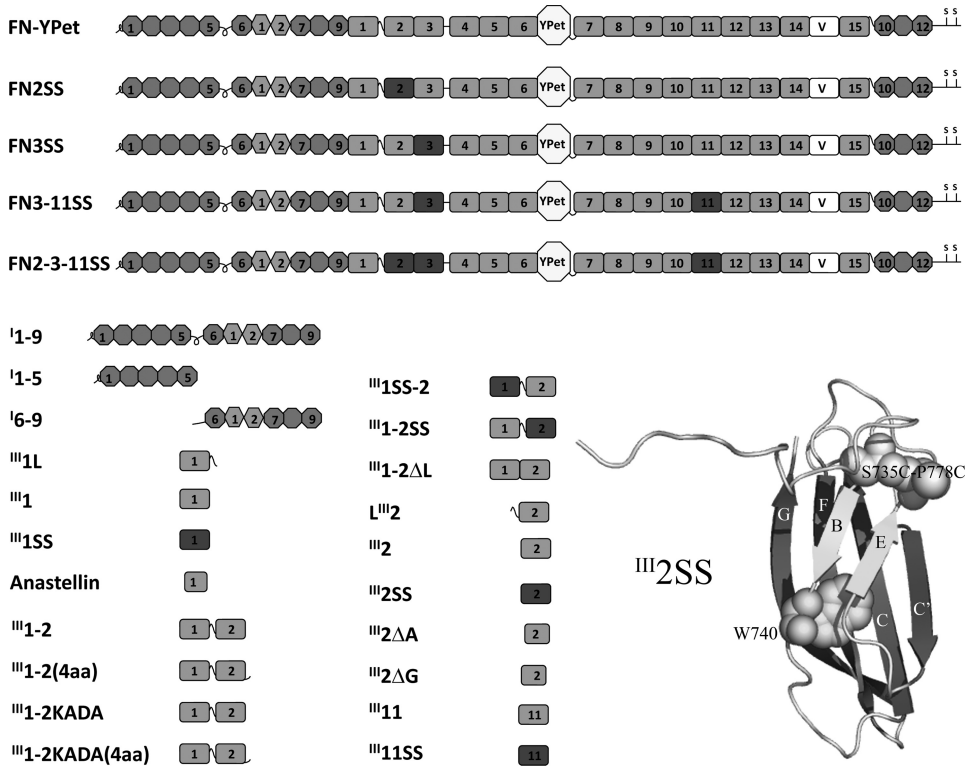

FIGURE 1. **Recombinant FN-YPet, FN fragments, and mutants used in this study.** FN-YPet has mYPet inserted between ^{III}6 and ^{III}7. The variable domain (*V*) is full length: 120 amino acids. FN2SS, FN3SS, FN3–11SS, and FN2–3-11SS have disulfide bonds incorporated into the designated domains in FN-YPet. The ^{I}1–9, ^{I}6–9, and ^{I}1–5 fragments and anastellin have a C-terminal His tag. The rest of the FN fragments have an N-terminal His tag. ^{III}1L and L^{III}2 are ^{III}1 and ^{III}2 with the 18-amino acid linker. ^{III}1–2KADA is ^{III}1–2 with K669A and D767A mutations. ^{III}1–2(4aa) and ^{III}1–2KADA(4aa) have an extra four amino acids at the C termini. ^{III}1SS, ^{III}1SS-2, ^{III}2SS, ^{III}1–2SS, and ^{III}11SS have engineered disulfide bonds. ^{III}1–2ΔL is ^{III}1–2 with the 14 amino acids of the linker deleted. ^{III}2ΔA is ^{III}2 with the A strand deleted, and ^{III}2ΔG is ^{III}2 with the G strand deleted. The tryptophan and engineered disulfide bond are indicated in the ^{III}2SS structure, which was created by the PyMol computer program (Schrödinger) after modeling the disulfide mutations with SWISS-MODEL.

is inserted between ^{III}6 and ^{III}7) was also cloned into the pHLSec2 vector without adding the C-terminal His tag. The full-length FN disulfide mutants, FN2SS, FN3SS, FN3–11SS, and FN2–3-11SS, were generated by site-directed mutagenesis of FN-YPet. Purified expression vectors were transfected into HEK293T cells with polyethylenimine (25-kDa branched; Aldrich) as reported previously (40). To avoid exogenous FN contamination from serum, the serum-free medium Hybridoma SFM (Invitrogen) was used for transfection and expression. HEK293T produces a negligible amount of endogenous FN. The conditioned medium was collected after 4–6 days of transfection. ^{I}1–9 and ^{I}1–5 were purified with a cobalt column using imidazole, whereas FN-YPet and the disulfide mutants were purified with a gelatin column using 4 M urea for elution. To exchange the buffer, purified proteins were run through a PD-10 column (Amersham Biosciences), which was equilibrated with TBS or PBS. We also tried to express ^{I}6–9, but it suffered from proteolysis during expression. Because ^{I}1–9 and ^{I}6–9 were expressed in the same system, a protease-sensitive site in ^{I}6–9 is probably protected in ^{I}1–9. Therefore, ^{I}6–9 was generated from purified ^{I}1–9 by plasmin digestion. Plasmin cleaves at the C terminus of arginine 259, which is located between domains ^{I}5 and ^{I}6 (2). 5 μM ^{I}1–9 was digested with 10 μg/ml plasmin at room temperature overnight. The digestion was quenched with 2 mM PMSF, and then ^{I}6–9 was purified by passage over the cobalt column as described above.

Pelleting Assay—The proteins of interest were mixed in a final volume of 25 μl with TBS or PBS containing 5 mM EDTA and incubated at room temperature for ~16 h. After incubation, the samples were centrifuged at 20,000 × *g* for 10 min, and the supernatants were collected. The pellets were rinsed with 100 μl of TBS or PBS and resuspended with SDS-PAGE loading buffer. SDS-PAGE (15%) was performed using standard procedures.

Fluorescence Measurements—Fluorescence measurements were performed with a Shimadzu RF-5301-PC spectrofluorometer (37). For intrinsic tryptophan fluorescence measurements, 1 μM purified single FNIII domains in PBS were excited at 280 nm in the presence of 0–8 M urea, and emission spectra were recorded at 1-nm intervals from 300 to 400 nm with slit widths of 3 nm for excitation and 5 nm for emission. These measurements were carried out with triplicate samples at room temperature.

For 8-anilino-1-naphthalene sulfonate (ANS) fluorescence measurements, samples that contained 50 μM ANS and combinations of 10 μM anastellin and 10 μM FNIII domains or the disulfide mutants were excited at 360 nm, and emission spectra were recorded at 1-nm intervals from 370 to 620 nm using slit widths of 5 nm for both excitation and emission. The measurements for the disulfide mutants were performed with or without 1 mM DTT.

For FRET measurements, 1 μM samples were excited at 433 nm, and emission spectra were recorded at 1-nm intervals from 440 to 620 nm using slit widths of 3 nm for both excitation and emission. These measurements were done with quadruplicate

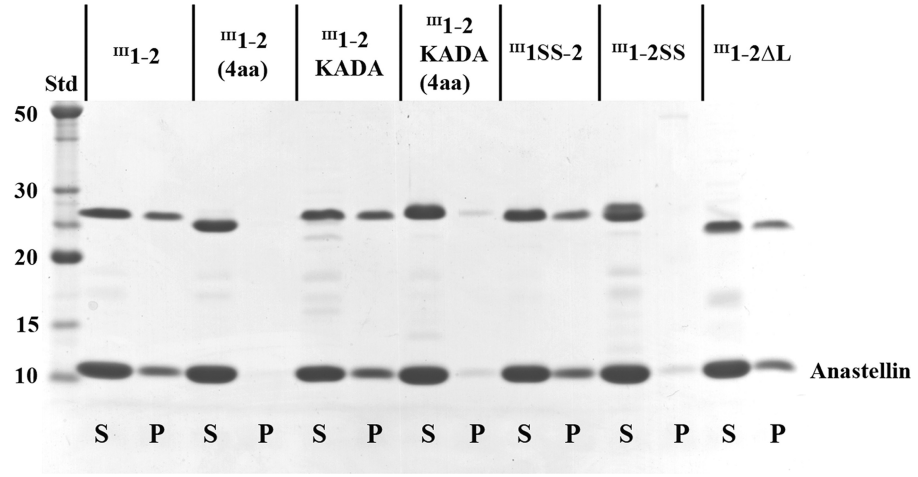

FIGURE 2. **SuperFN-like aggregation with the ^{II}1–2 mutants and anastellin.** 10 μM ^{III}1–2 mutants (~24 kDa) were mixed with 40 μM anastellin (~10 kDa) for ~16 h, and centrifuged at 20,000 × *g* for 10 min. *S*, supernatant; *P*, pellet; *Std*, BenchMark protein ladder (Invitrogen). The ^{III}1–2KADA, ^{III}1SS-2, and ^{III}1–2ΔL formed aggregates with anastellin, essentially the same as wild-type ^{II}1–2. In contrast, ^{III}1–2(4aa), ^{III}1–2KADA(4aa), and ^{III}1–2SS did not form any aggregates.

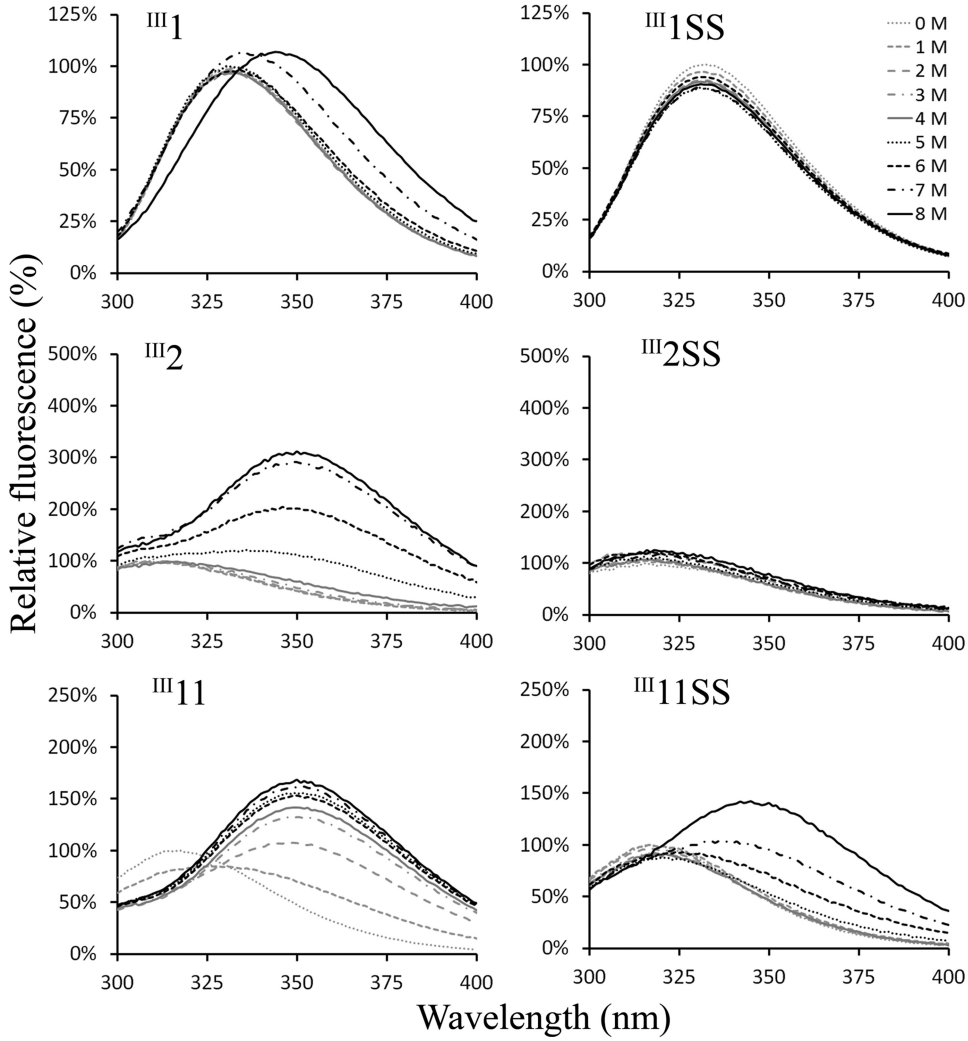

FIGURE 3. **The stability of ^{III}1, ^{III}2, ^{III}11, and the disulfide mutants.** The single FNIII domains were excited at 280 nm, and tryptophan fluorescence was recorded at wavelengths from 300 to 400 nm. Urea was used for denaturation. The emission intensity was normalized to that of the emission peak in 0 M urea. The engineered disulfide bonds significantly stabilized these domains.

samples at room temperature. Trypsin (10 μg/ml) digestion and ^{I}1–9 (2 μM) incubation were carried out for 1 h before measurements were made.

Gelatin Precipitation Assay—The proteins of interests were mixed in a final volume of 200 μl of PBS containing 5 mM EDTA and incubated for 1 h at room temperature. 30 μl of gelatin-

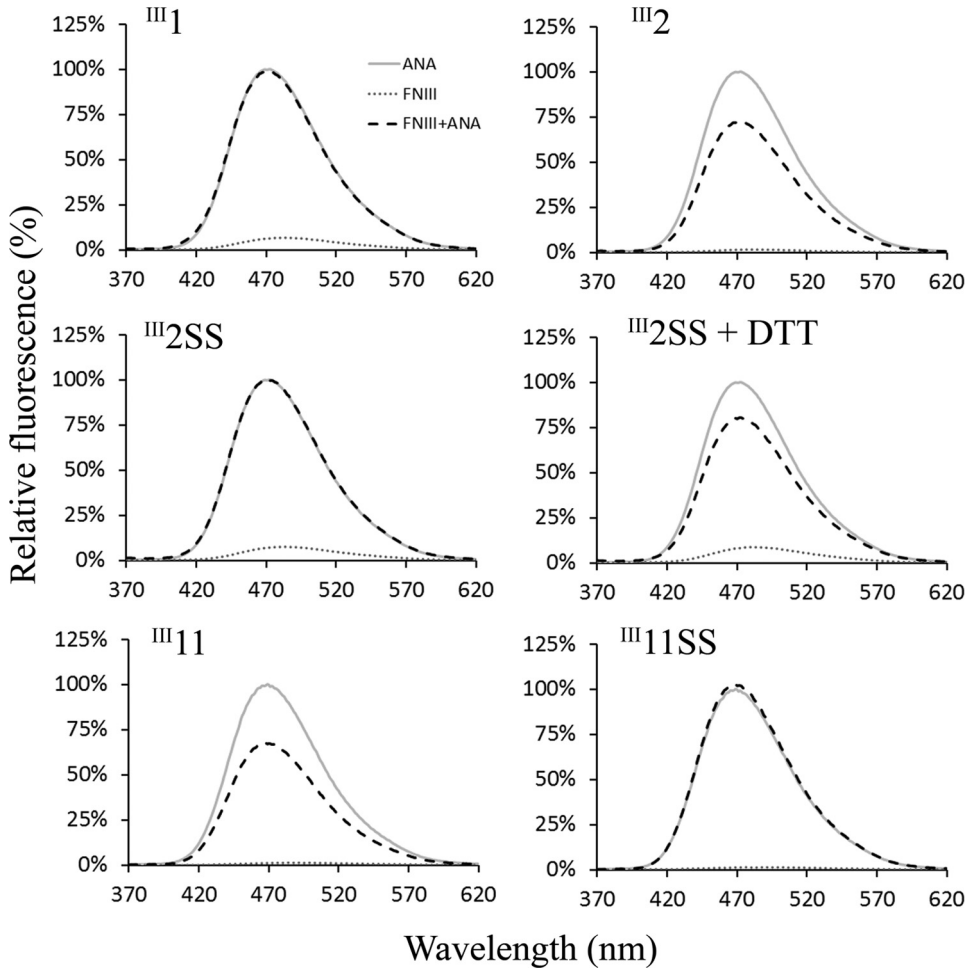

FIGURE 4. **FNIII domain binding to anastellin measured by ANS fluorescence.** 10 μM anastellin, 10 μM FNIII domains, and mixtures of anastellin and FNIII domains were mixed with 50 μM ANS. ANS fluorescence was recorded from 370 to 620 nm, with excitation at 360 nm. The emission intensity was normalized to that of the mixture of ANS and anastellin at 470 nm. ANS reacted with anastellin to enhance its fluorescence, but this was decreased by the presence of $^{III}2$ and $^{III}11$, indicating that these domains interacted with anastellin to reduce ANS binding. The disulfide bonds in $^{III}2$ and $^{III}11$ eliminated anastellin binding. Under reducing conditions, the disulfide mutants interacted with anastellin and led to a reduction in ANS fluorescence just like wild type.

agarose (Sigma) was added and incubated for an additional hour at room temperature. After incubation, the samples were centrifuged at 300 rpm for 1 min, and the supernatants were removed. The agarose beads were washed with 1 ml of PBS five times. The bound components were eluted from the beads with 30 μl of 8 M urea/PBS.

Glycerol Gradient Sedimentation and Gel Filtration Chromatography—We used glycerol gradient sedimentation to estimate the sedimentation coefficients. Wild-type $^{III}1$–2 and $^{III}1$–2KADA were sedimented on a 15–40% glycerol gradient in 0.2 M ammonium bicarbonate at 50,000 rpm for 16 h with a Beckman SW 55.1 rotor. Aldolase (7.3 S), BSA (4.6 S), ovalbumin (3.5 S), and cytochrome *c* (1.7 S) were used to calibrate the glycerol gradients.

The Stokes radii (R_s) of $^{III}1$–2 and $^{III}1$–2KADA were estimated by gel filtration on a Sephacryl S-100 column (GE Healthcare) at a flow rate of 1 ml/min. PBS was used for elution. The column was calibrated with BSA (R_s = 3.55 nm), ovalbumin (3.05 nm), and cytochrome *c* (1.41 nm).

Cell Culture and FN-YPet Quantification Using YPet Fluorescence—The FN($^{-/-}$) cell line 5F was kindly provided by Deane Mosher (University of Wisconsin). These cells were maintained with DMEM containing 10% FCS (Sigma). The cells were harvested with 0.05% trypsin, 2 mM EDTA (Invitrogen), after which 2 mM PMSF was added to quench the trypsin. The cells were rinsed with DMEM and resuspended with DMEM containing 1% FCS, which was depleted of FN by passage through a gelatin column. Cell suspensions (0.4 ml; 5×10^5 cells/ml) containing 30 nM FN-YPet with various FN fragments or FN2SS, FN3–11SS, or FN2–3-11SS were plated into a 24-well culture plate. The concentrations of FN-YPet and disulfide mutants were estimated from the absorbance at 514 nm with the molar extinction coefficient of monomeric YPet, 85,000 M^{-1} cm^{-1} (34). 12-mm circular coverglasses were added to several wells for microscopy. After the cells were cultured for ~16 h, each well was rinsed three times with 0.5 ml of PBS containing Ca^{2+} and Mg^{2+} and then treated with 0.1 ml of trypsin (10 μg/ml) in PBS containing 5 mM EDTA for 30 min at room temperature. Trypsin digestion was quenched with 2 mM PMSF, and samples were centrifuged at 15,000 rpm for 10 min to remove the cells. This solubilized most of the matrix, as indicated by the loss of almost all fluorescence in the light microscope. Total matrix FN-YPet was then determined from fluorescence of the supernatant. Samples were excited at 514 nm,

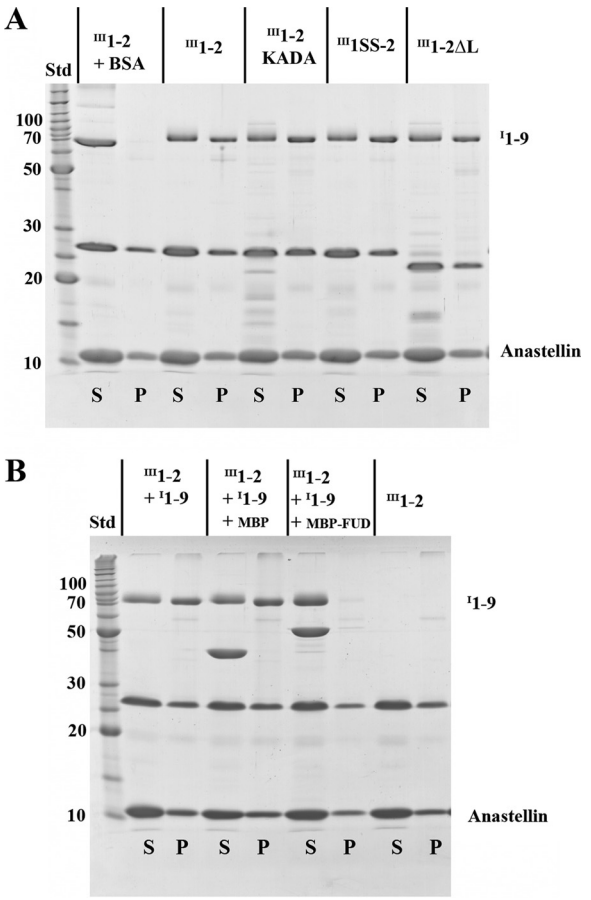

FIGURE 5. **^{I}1–9 co-precipitates with the superFN-like aggregates.** *A*, ^{I}1–9 co-precipitates with ^{III}1–2 mutants and anastellin. 10 μM ^{III}1–2 mutants plus 2 μM ^{I}1–9 (~70 kDa) or BSA were mixed with 40 μM anastellin. ^{I}1–9 was able to co-precipitate with all the ^{III}1–2 mutants/anastellin aggregates. BSA remained in the supernatant. *S*, supernatant; *P*, pellet; *Std*, BenchMark protein ladder (Invitrogen). *B*, FUD (bacterial adhesin) inhibits ^{I}1–9 co-precipitation with the aggregate. 10 μM ^{III}1–2 and 2 μM ^{I}1–9 were mixed with 40 μM anastellin. 2 μM MBP or MBP-FUD was also added to the reaction. MBP-FUD inhibited ^{I}1–9 co-precipitation with the ^{III}1–2/anastellin aggregate, but MBP did not.

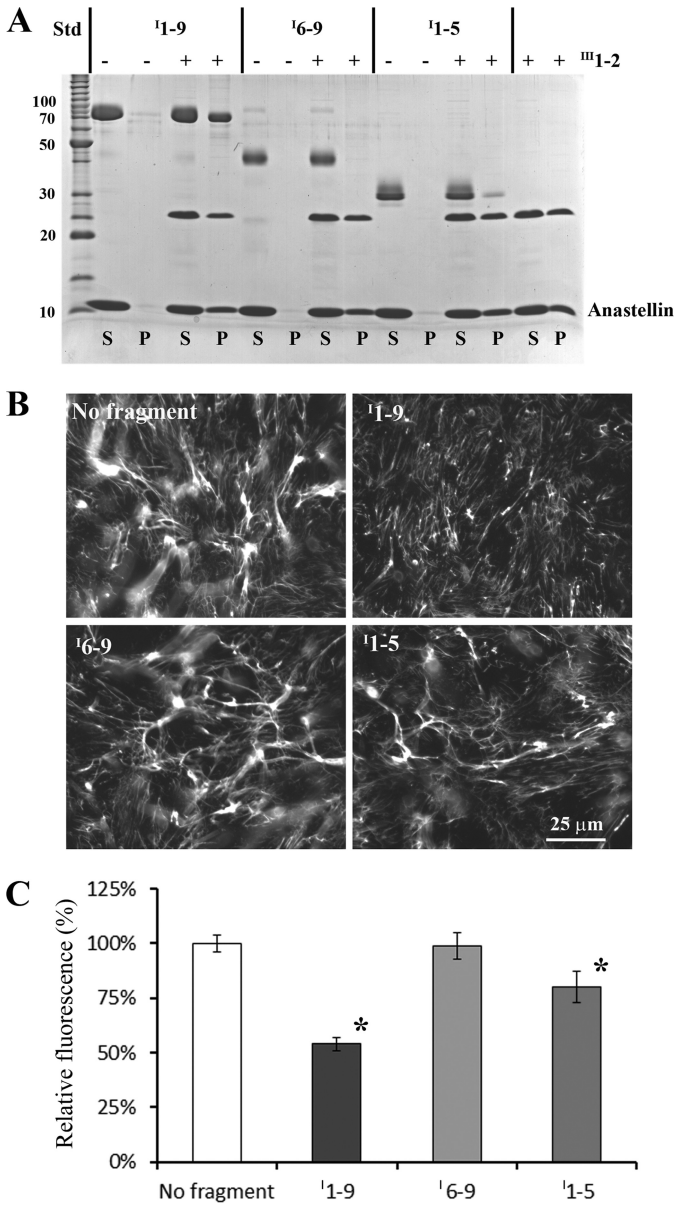

FIGURE 6. **Activities of ^{I}1–9, ^{I}6–9, and ^{I}1–5 for binding the ^{III}1–2/anastellin aggregate and inhibiting FN matrix formation.** *A*, for the pelleting assay, 2 μM ^{I}1–9, ^{I}6–9 (~40 kDa), or ^{I}1–5 (~30 kDa) was mixed with 40 μM anastellin, with or without 10 μM ^{III}1–2. A significant amount of ^{I}1–9 co-precipitated with the ^{III}1–2/anastellin aggregate. On the other hand, only a trace amount of ^{I}1–5 co-precipitated, and ^{I}6–9 did not co-precipitate at all. None of the fragments formed any aggregates with anastellin in the absence of ^{III}1–2. *S*, supernatant; *P*, pellet; *Std*, BenchMark protein ladder (Invitrogen). *B*, various FN fragments (1 μM) were added to FN($^{-/-}$) cell culture with FN-YPet (30 nM) and cultured for ~16 h. ^{I}1–9 inhibited FN matrix formation, ^{I}6–9 had no significant effect on FN matrix assembly, and ^{I}1–5 reduced the FN matrix. *C*, the amount of matrix FN was estimated by measuring YPet fluorescence after solubilizing YPet from cell culture by trypsin treatment. The emission intensity was normalized to that of a control sample (no fragment). ^{I}1–9 and ^{I}1–5 reduced the FN matrix by 50 and 20%, respectively. The *error bars* indicate standard deviation. *, $p < 0.01$.

and emission spectra were recorded at 528 nm using slit widths of 3 nm for excitation and 5 nm for emission. These measurements were carried out with quadruplicate samples at room temperature. Note that mild trypsin digestion does not affect YPet fluorescence (34). For microscopy, the samples were fixed with 3.7% formaldehyde in PBS, washed, and mounted on slides. The samples were observed with a light microscope (Zeiss Axiophot), and the images were captured with a cooled charge-coupled device camera (CoolSNAPHQ; Roper Scientific).

RESULTS

SuperFN-like Aggregation from ^{III}1–2: Search for Blocking Mutants—The recombinant proteins used in this study are diagrammed in Fig. 1. We have previously shown that a disulfide bond introduced into ^{III}3, locking the B strand to the E strand, inhibited anastellin binding (37). Here we have introduced the equivalent disulfide bond into domains ^{III}1, ^{III}2 (Fig. 1), and ^{III}11. We have also previously shown that the whole FN molecule is not needed for superFN formation; a small FN fragment, ^{III}1–2, forms a superFN-like aggregate when mixed with anastellin (24). In addition to these disulfide locks, we have investigated mutants ^{III}1–2KADA, and ^{III}1–2ΔL in which 14 amino acids were deleted from the 18-amino acid linker between ^{III}1 and ^{III}2. Two additional mutants, ^{III}1–2/4aa and ^{III}1–2KADA/4aa, have a four-amino acid extension (the first four amino acids of ^{III}3) at the C terminus of ^{III}2, which significantly

improved the solubility of these proteins. Similar C-terminal extensions are known to stabilize other FNIII domains (41, 42).

We tested these constructs for ability to assemble a superFN-like aggregate, using a pelleting assay (Fig. 2). Our preliminary study indicated that 40 μM anastellin was required to efficiently precipitate 10 μM ^{III}1–2 (supplemental Figs. S1 and S2). The four-amino acid extension on the C terminus of ^{III}1–2 completely suppressed superFN-like aggregation, suggesting that the stability of ^{III}2 is a key factor in aggregation. In full-length FN, those four amino acids are probably incorporated into ^{III}3 and thus would not lead to stabilization of ^{III}2. In fact, in our previous study, fragments containing both ^{III}2 and ^{III}3 (^{III}1–3 and ^{III}1–5) were able to form superFN-like aggregates (24). The KADA mutations had no effect on aggregation. The disulfide lock in ^{III}1 had no effect, whereas the disulfide in ^{III}2 completely blocked aggregation. Removing the linker had no effect. Overall, these data are consistent with the interpretation that instability and opening of ^{III}2 is essential for superFN-like aggregation of ^{III}1–2.

We then tested the stability of FNIII domains ^{III}1, ^{III}2, and ^{III}11 to chemical denaturation. ^{III}11 was included because it was previously found to bind anastellin (24). Intrinsic tryptophan fluorescence was used to examine the stability of the single FNIII domains in the presence of urea. All FNIII domains of FN have a conserved buried tryptophan as shown in Fig. 1. ^{III}1 has two additional tryptophans, one of which is exposed on the surface. A broad emission peak for ^{III}1, centered near 330 nm under physiological conditions, was shifted toward 350 nm at urea concentrations 7 and 8 M (Fig. 3). The emission peak for ^{III}2 near 310 nm was shifted toward 350 nm, and the intensity was increased at urea concentrations above 5 M. The emission peak for ^{III}11 near 310 nm was shifted toward 350 nm, and the intensity was increased at urea concentrations above 1 M. ^{III}11 is the weakest domain among the FNIII domains we have tested. In contrast, the disulfide mutants, ^{III}1SS and ^{III}2SS, were quite stable against urea denaturation (Fig. 3), as previously reported for ^{III}3SS (37). ^{III}11SS was also stabilized by the disulfide bond relative to wild-type ^{III}11, although it was still denatured by 6 M urea.

Anastellin binding to these FNIII domains was analyzed by ANS fluorescence. We previously found that the reactivity of ANS to anastellin was reduced when anastellin formed a complex (37). The emission intensity of ANS with FNIII domains alone was negligible (Fig. 4), consistent with these domains being folded properly with no exposed hydrophobic patches that could interact with ANS. On the other hand, the emission intensity of ANS was dramatically increased when added to anastellin, with an emission maximum of ~470 nm. In the presence of ^{III}2 or ^{III}11, the emission intensity was significantly reduced (Fig. 4), whereas ^{III}1, ^{III}1SS, ^{III}2SS, and ^{III}11SS had no effect, indicating that there was no interaction with anastellin. In the presence of DTT, however, ^{III}2SS and ^{III}11SS were able to reduce the emission intensity like wild-type ^{III}2 and ^{III}11.

Binding of ^{I}1–9 to ^{III}1–2—Because ^{I}1–9, which is one of the matrix assembly sites, interacted with superFN (24), we examined whether ^{I}1–9 can bind the ^{III}1–2/anastellin aggregate. Indeed, ^{I}1–9 was co-precipitated not only with the wild-type ^{III}1–2 aggregate but also with ^{III}1–2KADA, ^{III}1SS-2, and ^{III}1–2ΔL mutants (Fig. 5*A*). These results suggest that the presence of the linker or unfolding of ^{III}1 does not contribute to ^{I}1–9 binding. The specificity of ^{I}1–9 binding to the aggregate was also confirmed by inhibition with FUD (Fig. 5*B*), a 49-amino acid peptide from a bacterial adhesin that is known to bind ^{I}1–9 with high affinity (43, 44).

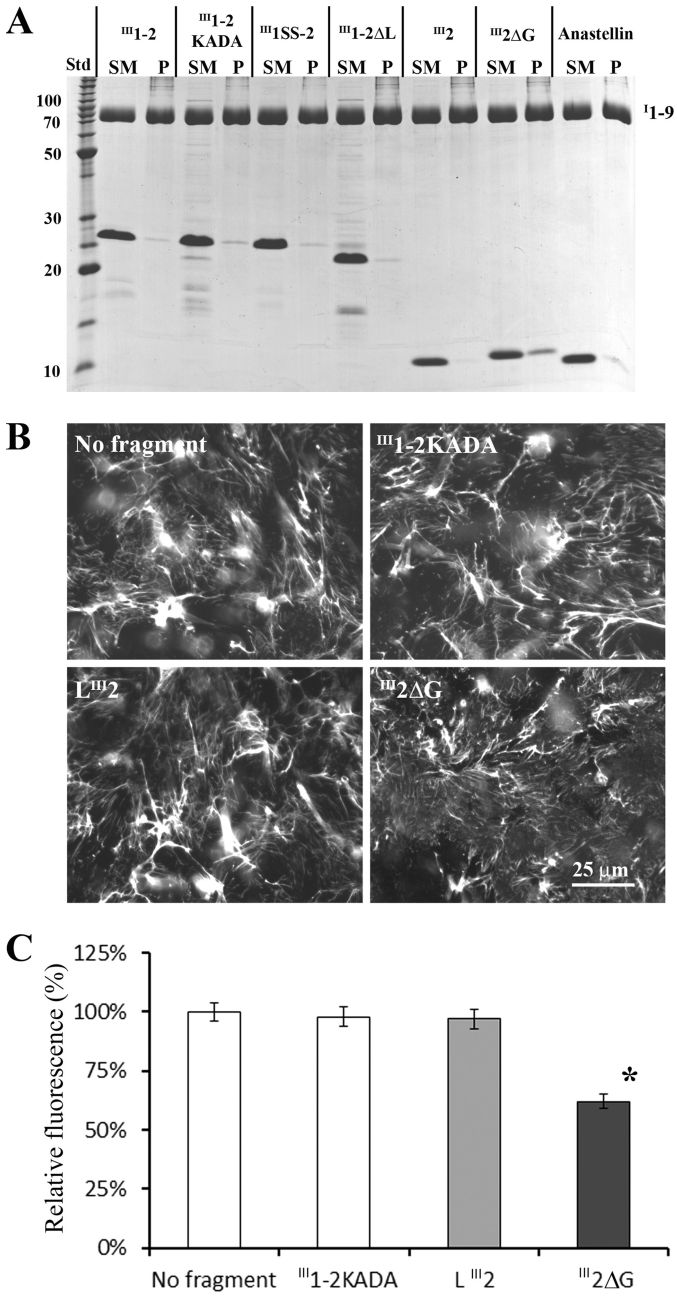

FIGURE 7. **^{III}2ΔG interacts with ^{I}1–9 and is able to inhibit FN matrix formation.** *A*, for the gelatin precipitation assay, 10 μM ^{III}1–2, ^{III}1–2KADA, ^{III}1SS-2, ^{III}1–2ΔL, ^{III}2, ^{III}2ΔG, or anastellin was mixed with 2 μM ^{I}1–9 and then incubated with gelatin-agarose beads. None of the fragments were pulled down with ^{I}1–9 except for ^{III}2ΔG, indicating that only ^{III}2ΔG was able to bind ^{I}1–9. *SM*, starting material; *P*, pellet; *Std*, BenchMark protein ladder (Invitrogen). *B*, various FN fragments (1 μM) were added to the FN($^{-/-}$) cell culture with FN-YPet (30 nM). ^{III}2ΔG inhibited FN matrix formation. ^{III}1–2KADA and L^{III}2 had no effect on FN matrix assembly. *C*, the amount of matrix FN was estimated by measuring YPet fluorescence after solubilizing YPet from cell culture by trypsin treatment. ^{III}2ΔG inhibited the FN matrix by 40%. The *error bars* indicate standard deviation. *, $p < 0.01$.

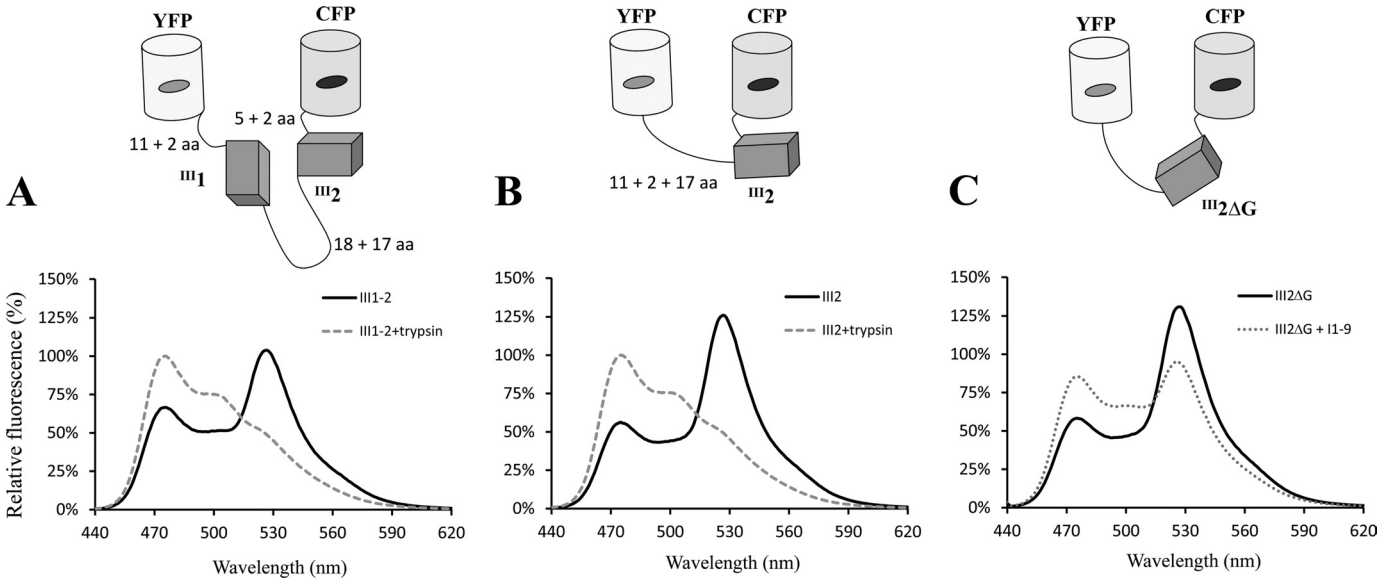

FIGURE 8. **Diagrams and emission spectra of the FRET constructs.** The C-terminal 11-amino acid segment of YFP and the N-terminal 5-amino acid segment of CFP are presumably unstructured (34). The N-terminal 17-amino acid region of $^{III}2$ and the 18-amino acid linker between $^{III}1$ and $^{III}2$ are also unstructured. *A* and *B*, samples with and without trypsin treatment were excited at 433 nm, and emission intensity was recorded at wavelengths from 440 to 620 nm. *C*, addition of $^{I}1–9$ to FRET($^{III}2\Delta G$) significantly reduced the FRET signal (this is not a trypsin treatment, but a comparison of spectra with and without $^{I}1–9$). *aa*, amino acids.

TABLE 1
FRET signals of $^{III}1–2$, III2, and mutants

	FRET efficiency	Emission ratio
III1–2	0.33	1.55
III1–2KADA	0.33	1.56
III2	0.44	2.23
III2ΔG	0.41	2.23
III2ΔG + I1–9	0.15	1.09
$^{III}2\Delta G$ + I1–9 + MBP	0.14	1.07
$^{III}2\Delta G$ + I1–9 + MBP-FUD	0.42	2.22

We also tested the two smaller fragments of $^{I}1–9$, $^{I}1–5$ and $^{I}6–9$, for the ability to bind the $^{III}1–2$/anastellin aggregate (Fig. 6*A*). Only a trace amount of $^{I}1–5$ co-precipitated, whereas $^{I}6–9$ did not co-precipitate at all. We then tested the ability of $^{I}1–9$ and its two fragments to inhibit FN matrix assembly in cell culture. Fluorescence microscopy showed that $^{I}1–9$ inhibited FN matrix formation as reported previously (19, 23, 24). The partial inhibition of matrix assembly in the present study is less than the almost complete inhibition in our previous study (24), probably because of the different cell type and culture conditions, including the lower concentration of $^{I}1–9$. $^{I}1–5$ reduced the matrix, whereas $^{I}6–9$ had no effect on FN matrix assembly (Fig. 6*B*).

To quantitate the matrix, we measured the YFP fluorescence released into the soluble fraction after trypsin treatment (Fig. 6*C* and supplemental Fig. S3). $^{I}1–9$ reduced the FN matrix by 50%, $^{I}6–9$ had no significant effect on FN matrix assembly, and $^{I}1–5$ decreased the matrix by 20%. These results showed that the longer segment, $^{I}1–9$, has stronger binding to the superFN-like aggregate and a more inhibitory effect on FN matrix formation than either of the shorter fragments.

Because $^{I}1–9$ is capable of binding gelatin through the $^{I}6–9$ region (45), we used a gelatin precipitation assay to study the interaction between $^{I}1–9$ and several FN fragments. Before using this assay, we verified that gelatin (~5%) had no effect on FN matrix formation when added to cell culture. An earlier study showed that fluorescently labeled gelatin is able to stain FN matrix fibrils (46), indicating that the gelatin binding sites are not blocked by matrix assembly. In the gelatin precipitation assay, $^{III}1–2$ and its mutants did not co-precipitate with $^{I}1–9$ (Fig. 7*A*). This was surprising because $^{III}1–2$KADA was previously reported to bind $^{I}1–5$ and $^{I}1–9$ (32, 33). It is possible that gelatin binding blocks the interaction between $^{I}1–9$ and $^{III}1–2$KADA. We also added $^{III}1–2$KADA to cell culture, but it had no effect on FN matrix formation (Fig. 7, *B* and *C*, and supplemental Fig. S3). The only mutant that showed any binding to $^{I}1–9$ was $^{III}2\Delta G$, which is discussed below.

Structural analysis of $^{III}1–2$ and the KADA Mutant—The previously studied KADA mutant was reported to run far ahead of the wild-type $^{III}1–2$ on gel filtration and was thought to have a larger hydrodynamic radius (32). We therefore examined our $^{III}1–2$KADA by glycerol gradient sedimentation and gel filtration chromatography. Both wild-type $^{III}1–2$ and $^{III}1–2$KADA sedimented at ~1.9 S (supplemental Fig. S4) (S_{max}/S = 1.6, indicating a moderately extended protein (47)). Gel filtration chromatography on Sephacryl S-100 also showed that both proteins eluted at the same R_s, ~2.5 nm (data not shown).

We also examined the difference between $^{III}1–2$ and $^{III}1–2$KADA using FRET, repeating the analysis of Karuri *et al.* (33). Our FRET construct, FRET($^{III}1–2$), had mYPet and mECFP* on the N and C termini of $^{III}1–2$, as diagramed in Fig. 8*A*. The emission spectra of FRET($^{III}1–2$) with and without trypsin digestion are shown in Fig. 8*A*. The FRET signals were determined by FRET efficiency, which was calculated from the decreased donor emission at 475 nm and by the ratio of the acceptor emission at 528 nm to the donor emission at 475 nm (Table 1). Based on FRET efficiency and the Förster distance for this fluorophore pair (~5.3 nm), we estimated the distance between the two fluorophores in the FRET($^{III}1–2$) construct to

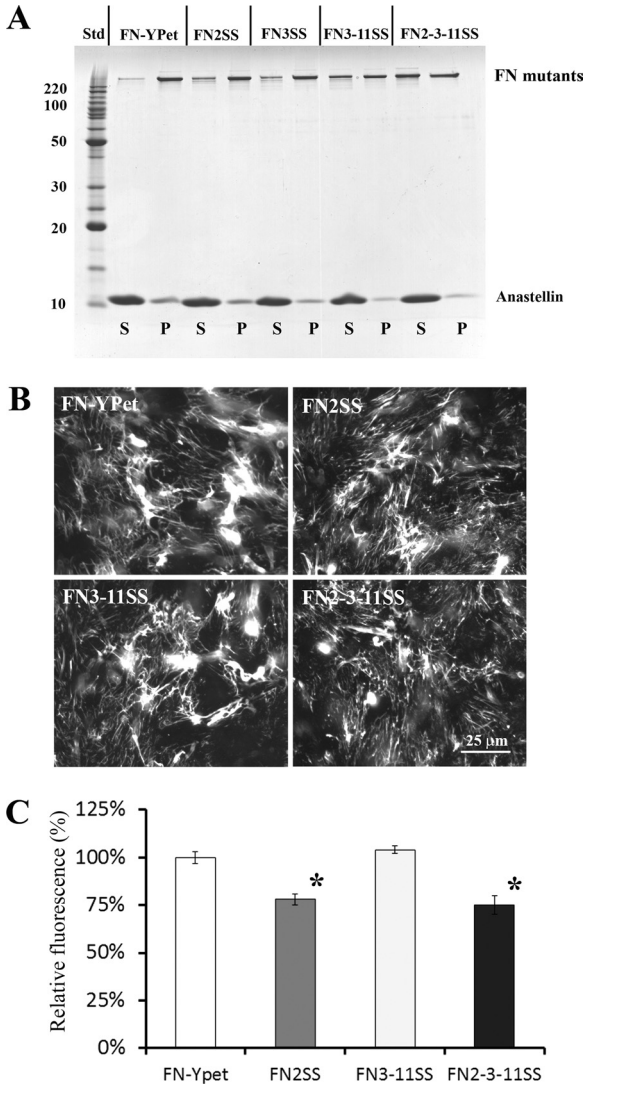

FIGURE 9. **Effects of engineered disulfide bonds in full-length FN on superFN aggregation and cellular matrix assembly.** *A*, 1 μM full-length FN-YPet (~280 kDa) or FN-YPet with the indicated disulfide mutations was mixed with 20 μM anastellin. FN2SS and FN3SS slightly reduced the aggregates. Disulfide bonds in both ^{III}3 and ^{III}11 (FN3–11SS) decreased the aggregate. Three disulfide bonds in ^{III}2, ^{III}3, and ^{III}11 (FN2–3-11SS) further reduced the aggregate. *S*, supernatant; *P*, pellet; *Std*, BenchMark protein ladder (Invitrogen). *B*, purified 30 nM FN-YPet, FN2SS, FN3–11SS, and FN2–3-11SS were added to FN($^{-/-}$) cell culture and cultured for ~16 h. Fluorescence microscopy showed that FN2SS and FN2–3-11SS assembled less FN matrix. *C*, the amount of matrix FN was estimated by measuring YPet fluorescence after solubilizing YPet from cell culture by trypsin treatment. FN2SS and FN2–3-11SS reduced the FN matrix by 20% relative to wild type. This suggests that FN2SS alone is the primary cause of the inhibitory effect. The *error bars* indicate the standard deviation. *, $p < 0.01$.

be ~6.0 nm. This is a reasonable value, because this construct contains flexible regions of ~55 amino acids in addition to the folded domains (see our previous study for details on distance estimation for intrinsically unstructured peptides from FRET efficiency (34). Our FRET signal was higher than that of Karuri's study (33). We expected that our FRET signal might be lower, because Karuri *et al.* used earlier versions of CFP and YFP that have a weak dimerizing activity, whereas we used monomeric versions (34). Their lower FRET might be attributed to their EYFP having a lower absorption or greater chloride sensitivity than the mYPet we used.

As expected from our hydrodynamics analysis, the signal of the FRET(^{III}1–2KADA) construct was identical to that of wild type (Table 1). These measurements were performed with PBS. We also tested Tris buffer (pH 7.4) and different salt concentrations (0, 0.2, and 0.5 M NaCl). There was no significant difference between the wild type and KADA mutant in any of these buffer conditions. High salt reduced the FRET signal for both constructs, but we have seen this effect in other FP-based FRET constructs, perhaps because high salt induces an extended conformation of the unstructured segment. The addition of ^{I}1–9 to either the FRET(^{III}1–2) or FRET(^{III}1–2KADA) construct had no effect on the FRET signals. Thus, we did not find any difference between wild type and the KADA mutant.

A Binding Site for ^{I}1–9 in Truncated ^{III}2ΔG—We also tested several small FN fragments (^{III}1L, L^{III}2, ^{III}1, ^{III}2) and anastellin in the gelatin precipitation assay. None of the fragments bound ^{I}1–9. Therefore, we postulated that a cryptic binding site for ^{I}1–9 in the ^{III}1–2/anastellin aggregate is located on ^{III}2 and only exposed when it unfolds to form the aggregate. To further explore this hypothesis, we generated destabilized ^{III}2 mutants by deleting the N- or C-terminal β strand. The strand A deletion (^{III}2ΔA) showed a spectrum similar to that of wild type in our tryptophan fluorescence assay (supplemental Fig. S5). This is consistent with a recent NMR study showing that the residues that make up strand A are unstructured (Fig. 1) (32) and thus not likely to affect folding. In the gelatin precipitation assay, ^{III}2ΔA also did not interact with ^{I}1–9. In contrast, in the strand G deletion (^{III}2ΔG), the broad tryptophan emission peak, which was ~340 nm in the absence of urea (*versus* 310 nm for ^{III}2 and ^{III}2ΔA), was shifted to 350 nm, and the intensity was increased even in 2 M urea (supplemental Fig. S5). These results indicate that the tryptophan in this mutant is more exposed to the solvent in 0 M urea and is easily denatured by mild urea treatment. Thus, ^{III}2ΔG appeared to be the destabilized mutant we wanted. In the gelatin precipitation assay, ^{III}2ΔG co-precipitated with ^{I}1–9 (Fig. 7*A*), suggesting that the binding site for ^{I}1–9 is exposed within this truncated ^{III}2 domain. ^{III}2ΔG did not co-precipitate with ^{I}6–9.

We further studied the interaction between ^{III}2ΔG and ^{I}1–9 using FRET. The control construct, FRET(^{III}2), showed a strong FRET signal (Fig. 8*B* and Table 1), and FRET(^{III}2ΔG) was similar to wild type. Both constructs have a flexible region of ~37 amino acids in addition to the folded domain (17 amino acids for the unstructured A strand, 16 amino acids for the flexible regions of the FPs, plus four amino acids from cloning sites (see Ref. 34 for details of this calculation). The longer flexible region might bring the two FPs close together, because these FRET signals were higher than those we measured previously for inserts of single FNIII domains ^{III}3 and ^{III}10 (34). The separation of the two fluorophores was estimated to be ~5.5 nm. This distance fits to that of intrinsically unstructured peptides with similar lengths (34). The addition of ^{I}1–9 to the FRET(^{III}2) construct had no effect on the FRET signal. In contrast, the signal of FRET(^{III}2ΔG) was greatly decreased by the addition of ^{I}1–9 (Fig. 8*C* and Table 1), suggesting that ^{I}1–9 binding induced an extended conformation of ^{III}2ΔG. ^{I}1–9 binding to the FRET(^{III}2ΔG) construct was inhibited by FUD (Table 1). When ^{III}2ΔG was tested in cell culture, it was able to inhibit FN matrix

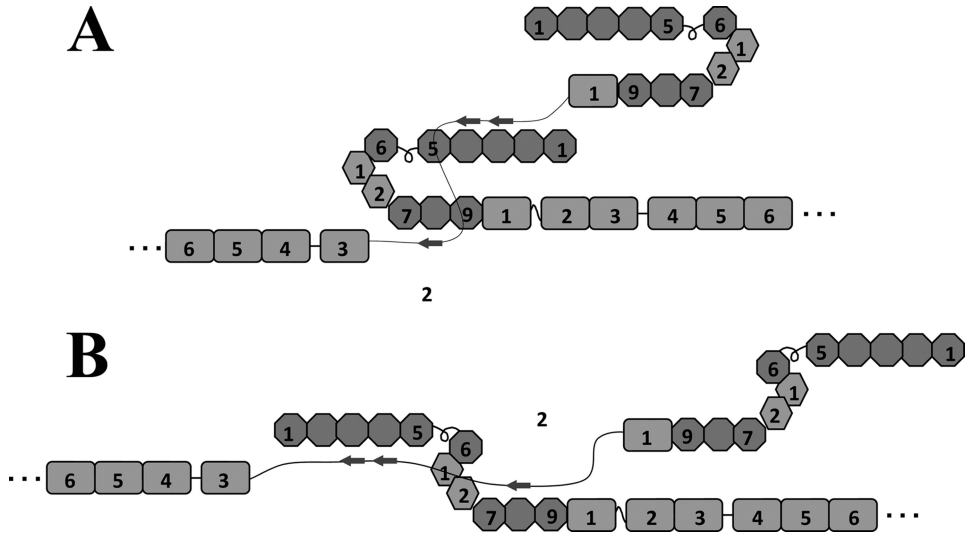

FIGURE 10. **Hypothetical models of the interaction between $^{I}1–9$ and unfolded $^{III}2$.** The diagram shows two possible models for how unfolded $^{III}2$ might interact with $^{I}1–9$ by forming tandem β strands that add to the FNI domains. $^{I}1–9$ could be in either a compact (*A*) or an extended (*B*) conformation.

formation by ~40% (Fig. 7, *B* and *C*, and supplemental Fig. S3), almost as much as the ~50% inhibition by I1–9 (Fig. 6*C*).

Disulfide Locks Partially Disrupt FN Matrix Assembly in Cell Culture—Based on our present and previous results, the unfolding of FNIII domains appears to be crucial for aggregation and assembly. Therefore, we engineered several disulfide mutations in full-length FN to test our findings. The qualities of purified proteins are shown in supplemental Fig. S6. Surprisingly, the single disulfide bond in $^{III}2$ (FN2SS) or $^{III}3$ (FN3SS) had only a slight effect on superFN aggregation (Fig. 9*A*). Two disulfide bonds, in $^{III}3$ and $^{III}11$ (FN3–11SS), decreased the aggregate a bit more, whereas three disulfide bonds, in $^{III}2$, $^{III}3$, and $^{III}11$ (FN2–3-11SS), greatly reduced aggregation but did not inhibit it completely. In the aggregate formed by FN2–3-11SS, the amount of anastellin was greatly reduced, indicating that the disulfides decrease anastellin binding. So how does the triple mutant even form the aggregate? It may have another anastellin binding site, or the disulfide locks may not block anastellin binding completely. In any case, these results suggest that the unfolding of $^{III}2$, $^{III}3$, and $^{III}11$ is important for superFN aggregation in full-length FN.

We also tested the full-length FN disulfide mutants in cell culture to see whether they could form a matrix. The disulfide bonds in $^{III}2$ (FN2SS and FN2–3-11SS) decreased the FN matrix by ~20% relative wild-type FN and FN3–11SS (Fig. 9, *B* and *C*, and supplemental Fig. S7). The ability of $^{III}2$ to unfold appears to be a factor but not indispensable for FN matrix assembly.

DISCUSSION

The importance of FNIII domain unfolding was originally pointed out by Litvinovich *et al.* (48), who discovered that individually expressed $^{III}9$ was very unstable and easily formed an amyloid-like aggregate. Another example was provided by recent reports that $^{III}3$ spontaneously unfolds and binds anastellin, a mechanism that seems important for initiating or forming superFN aggregation (24, 37, 49). In the present study, we discovered that the instability of $^{III}2$ was also important for superFN-like aggregation of the small fragment $^{III}1–2$. Moreover, the disulfide mutations in full-length FN verified that the instability of FNIII domains plays a role in superFN aggregation. In the case of FN matrix formation, the disulfide lock in $^{III}2$ caused a 20% reduction of matrix, whereas the locks in $^{III}3$ and $^{III}11$ had no effect. This is consistent with the previous demonstration that FN lacking $^{III}2$ was still able to assemble the matrix, although it was reduced somewhat (26). These findings suggest that the interaction between $^{I}1–9$ and $^{III}2$ is not essential for matrix assembly but is one of several redundant binding interactions between FN molecules. The $^{I}1–5$ deletion (20) or $^{I}1–9$ deletion[3] of full-length FN eliminates its ability to form the matrix, suggesting that $^{I}1–9$ has more than one assembly site and may be involved in all FN-FN interactions. It is also possible that $^{I}1–9$ plays another role in assembly such as binding to a cell surface receptor (possibly an integrin) (9, 50–52).

The $^{III}1–2$KADA mutant was first designed and characterized by Vakonakis *et al.* (32). They reported that wild-type $^{III}1–2$ eluted from a gel filtration column ahead of a 29-kDa standard, whereas the KADA mutant migrated in the void volume, ahead of a 150-kDa standard. We determined an R_s of 2.5 nm for both the wild type and KADA mutant, and both proteins sedimented identically at ~1.9 S (supplemental Fig. S4). As a quality check, we used a simplified Siegel-Monte calculation (47), $M = 4{,}205\ S\ R_s$, to determine a mass of 20 kDa, which is close to the actual mass of the protein, ~24 kDa. Our FRET constructs also did not show any significant difference between the wild type and the KADA mutant. We thus found no evidence for a conformational change induced by the KADA mutations. Vakonakis *et al.* (32) also reported that the KADA mutant, but not the wild type, had a high affinity for $^{I}1–5$. We found no binding to the larger $^{I}1–9$ by the gelatin precipitation assay or by FRET analysis.

The results of Karuri *et al.* (33), who studied the conformation of $^{III}1–2$ by FRET, add additional contradictions. In their

[3] T. Ohashi and H. P. Erickson, unpublished observation.

study, the KADA mutations enhanced the FRET signal, suggesting that the KADA mutant has a more compact conformation than that of wild type. This is the opposite of the Vakonakis model (32). However, their KADA mutant appeared to bind $^{I}1–9$, as shown by a reduction in the FRET signal. We found no change in FRET with $^{I}1–9$ and therefore no indication of binding. Three laboratories used slightly different constructs and methods to analyze the $^{III}1–2$KADA mutants, so they may not be directly comparable. The apparent contradictions are not subtle, but we have not been able to suggest a resolution. In our hands the KADA mutations have no effect on conformation or activity.

FNI domains are known to interact with intrinsically unstructured FN-binding proteins (FNBP, adhesins) on bacterial cell walls (43, 53, 54). The NMR structure of a complex between $^{I}1–2$ and FNBP from *Streptococcus dysgalactiae* showed that the unstructured FNBP formed additional tandem β strands on the FNI domains, a structure designated as a "tandem β-zipper" (53). The crystal structures of FNBP from *Staphylococcus aureus* also showed a tandem β strand arrangement with FNI domains (54). A similar structure containing additional β strands was reported recently in a complex of $^{I}8–9$ and type I collagen α1 chain (55). We found that domain $^{III}2$, destabilized by deletion of the G strand, bound to $^{I}1–9$, and the binding was completely inhibited by a bacterial adhesin (FUD) (Table 1). Although there are no direct structural data for the FUD-$^{I}1–9$ complex, circular dichroism and modeling suggested that the FUD bound by β strand addition (44). Therefore, we speculate that the binding of unfolded $^{III}2$ to $^{I}1–9$ may use a tandem β-zipper mechanism similar to known adhesins.

The binding to $^{I}1–9$ appeared to be stronger than to the shorter $^{I}1–5$ or $^{I}6–9$. The FNBP of *S. pyogenes* also bound more tightly to $^{I}1–9$ than to $^{I}1–5$ (43, 44, 56). Because $^{I}1–9$ is stable against proteolysis in comparison with $^{I}6–9$ (see "Experimental Procedures" for details), the longer $^{I}1–9$ may form a compact conformation that masks a protease-sensitive site. This model is also supported by the hairpin structure of the $^{I}6$-$^{II}2$ fragment (57). Structural studies of FN-FNBP complexes indicate that ~10 amino acids are required to form a β strand in a complex with one FNI domain (54, 55). We did not find any obvious sequence similarity between $^{III}2$ and adhesins. $^{III}2$ is composed of 93 amino acids ($^{III}2\Delta G$ is 82 amino acids) and theoretically could bind nine FNI domains, if fully unfolded. We do not know the structure of the $^{III}2$ domain in the $^{III}1–2$/anastellin aggregate, but the observation that it can bind $^{I}1–9$ suggests that some stretch of unfolded $^{III}2$ peptide may be available to form tandem β-zippers with the FNI domains. Multiple β-zippers might be made with either a compact conformation of $^{I}1–9$ (Fig. 10*A*) or an extended conformation (Fig. 10*B*).

Acknowledgments—We thank Dr. Deane Mosher (University of Wisconsin) for the generous gift of FN($^{-/-}$) cells, Dr. Bianca Tomasini-Johansson (University of Wisconsin) for the FUD construct, and Dr. Dan Leahy (Johns Hopkins University) for the pHLSce2 mammalian cell expression vector.

REFERENCES

1. Hynes, R. O. (1990) *Fibronectins*, Springer-Verlag, New York
2. Petersen, T. E., Thøgersen, H. C., Skorstengaard, K., Vibe-Pedersen, K., Sahl, P., Sottrup-Jensen, L., and Magnusson, S. (1983) *Proc. Natl. Acad. Sci. U.S.A.* **80,** 137–141
3. Kornblihtt, A. R., Umezawa, K., Vibe-Pedersen, K., and Baralle, F. E. (1985) *EMBO J.* **4,** 1755–1759
4. An, S. S., Jiménez-Barbero, J., Petersen, T. E., and Llinás, M. (1992) *Biochemistry* **31,** 9927–9933
5. Kar, L., Lai, C. S., Wolff, C. E., Nettesheim, D., Sherman, S., and Johnson, M. E. (1993) *J. Biol. Chem.* **268,** 8580–8589
6. Wu, C., Keivens, V. M., O'Toole, T. E., McDonald, J. A., and Ginsberg, M. H. (1995) *Cell* **83,** 715–724
7. Wennerberg, K., Lohikangas, L., Gullberg, D., Pfaff, M., Johansson, S., and Fässler, R. (1996) *J. Cell Biol.* **132,** 227–238
8. Sechler, J. L., Cumiskey, A. M., Gazzola, D. M., and Schwarzbauer, J. E. (2000) *J. Cell Sci.* **113,** 1491–1498
9. Takahashi, S., Leiss, M., Moser, M., Ohashi, T., Kitao, T., Heckmann, D., Pfeifer, A., Kessler, H., Takagi, J., Erickson, H. P., and Fässler, R. (2007) *J. Cell Biol.* **178,** 167–178
10. Pankov, R., Cukierman, E., Katz, B. Z., Matsumoto, K., Lin, D. C., Lin, S., Hahn, C., and Yamada, K. M. (2000) *J. Cell Biol.* **148,** 1075–1090
11. Ohashi, T., Kiehart, D. P., and Erickson, H. P. (2002) *J. Cell Sci.* **115,** 1221–1229
12. Dzamba, B. J., Jakab, K. R., Marsden, M., Schwartz, M. A., and DeSimone, D. W. (2009) *Dev. Cell* **16,** 421–432
13. Hynes, R. O., and Destree, A. (1977) *Proc. Natl. Acad. Sci. U.S.A.* **74,** 2855–2859
14. Yamada, K. M., Schlesinger, D. H., Kennedy, D. W., and Pastan, I. (1977) *Biochemistry* **16,** 5552–5559
15. Keski-Oja, J., Mosher, D. F., and Vaheri, A. (1977) *Biochem. Biophys. Res. Commun.* **74,** 699–706
16. McConnell, M. R., Blumberg, P. M., and Rossow, P. W. (1978) *J. Biol. Chem.* **253,** 7522–7530
17. Chen, H., and Mosher, D. F. (1996) *J. Biol. Chem.* **271,** 9084–9089
18. Ohashi, T., and Erickson, H. P. (2009) *Matrix Biol.* **28,** 170–175
19. McKeown-Longo, P. J., and Mosher, D. F. (1985) *J. Cell Biol.* **100,** 364–374
20. Schwarzbauer, J. E. (1991) *J. Cell Biol.* **113,** 1463–1473
21. Morla, A., and Ruoslahti, E. (1992) *J. Cell Biol.* **118,** 421–429
22. Ichihara-Tanaka, K., Maeda, T., Titani, K., and Sekiguchi, K. (1992) *FEBS Lett.* **299,** 155–158
23. Wu, C., Keightley, S. Y., Leung-Hagesteijn, C., Radeva, G., Coppolino, M., Goicoechea, S., McDonald, J. A., and Dedhar, S. (1998) *J. Biol. Chem.* **273,** 528–536
24. Ohashi, T., and Erickson, H. P. (2005) *J. Biol. Chem.* **280,** 39143–39151
25. Chernousov, M. A., Fogerty, F. J., Koteliansky, V. E., and Mosher, D. F. (1991) *J. Biol. Chem.* **266,** 10851–10858
26. Sechler, J. L., Rao, H., Cumiskey, A. M., Vega-Colón, I., Smith, M. S., Murata, T., and Schwarzbauer, J. E. (2001) *J. Cell Biol.* **154,** 1081–1088
27. Maqueda, A., Moyano, J. V., Hernández Del Cerro, M., Peters, D. M., and Garcia-Pardo, A. (2007) *Matrix Biol.* **26,** 642–651
28. Santas, A. J., Peterson, J. A., Halbleib, J. L., Craig, S. E., Humphries, M. J., and Peters, D. M. (2002) *J. Biol. Chem.* **277,** 13650–13658
29. Ichihara-Tanaka, K., Titani, K., and Sekiguchi, K. (1995) *J. Cell Sci.* **108,** 907–915
30. Sottile, J., and Mosher, D. F. (1993) *Biochemistry* **32,** 1641–1647
31. Aguirre, K. M., McCormick, R. J., and Schwarzbauer, J. E. (1994) *J. Biol. Chem.* **269,** 27863–27868
32. Vakonakis, I., Staunton, D., Rooney, L. M., and Campbell, I. D. (2007) *EMBO J.* **26,** 2575–2583
33. Karuri, N. W., Lin, Z., Rye, H. S., and Schwarzbauer, J. E. (2009) *J. Biol. Chem.* **284,** 3445–3452
34. Ohashi, T., Galiacy, S. D., Briscoe, G., and Erickson, H. P. (2007) *Protein Sci.* **16,** 1429–1438
35. Morla, A., Zhang, Z., and Ruoslahti, E. (1994) *Nature* **367,** 193–196
36. Briknarová, K., Akerman, M. E., Hoyt, D. W., Ruoslahti, E., and Ely, K. R. (2003) *J. Mol. Biol.* **332,** 205–215

37. Ohashi, T., Augustus, A. M., and Erickson, H. P. (2009) *Biochemistry* **48,** 4189–4197
38. Tomasini-Johansson, B. R., Kaufman, N. R., Ensenberger, M. G., Ozeri, V., Hanski, E., and Mosher, D. F. (2001) *J. Biol. Chem.* **276,** 23430–23439
39. Ellman, G. L. (1959) *Arch. Biochem. Biophys.* **82,** 70–77
40. Aricescu, A. R., Lu, W., and Jones, E. Y. (2006) *Acta Crystallogr. D Biol. Crystallogr* **62,** 1243–1250
41. Hamill, S. J., Meekhof, A. E., and Clarke, J. (1998) *Biochemistry* **37,** 8071–8079
42. Niimi, T., Osawa, M., Yamaji, N., Yasunaga, K., Sakashita, H., Mase, T., Tanaka, A., and Fujita, S. (2001) *J. Biomol NMR* **21,** 281–284
43. Ozeri, V., Tovi, A., Burstein, I., Natanson-Yaron, S., Caparon, M. G., Yamada, K. M., Akiyama, S. K., Vlodavsky, I., and Hanski, E. (1996) *EMBO J.* **15,** 989–998
44. Maurer, L. M., Tomasini-Johansson, B. R., Ma, W., Annis, D. S., Eickstaedt, N. L., Ensenberger, M. G., Satyshur, K. A., and Mosher, D. F. (2010) *J. Biol. Chem.* **285,** 41087–41099
45. Katagiri, Y., Brew, S. A., and Ingham, K. C. (2003) *J. Biol. Chem.* **278,** 11897–11902
46. Hsieh, P., Segal, R., and Chen, L. B. (1980) *J. Cell Biol.* **87,** 14–22
47. Erickson, H. P. (2009) *Biol. Proced. Online* **11,** 32–51
48. Litvinovich, S. V., Brew, S. A., Aota, S., Akiyama, S. K., Haudenschild, C., and Ingham, K. C. (1998) *J. Mol. Biol.* **280,** 245–258
49. Vakonakis, I., Staunton, D., Ellis, I. R., Sarkies, P., Flanagan, A., Schor, A. M., Schor, S. L., and Campbell, I. D. (2009) *J. Biol. Chem.* **284,** 15668–15675
50. Hocking, D. C., Sottile, J., and McKeown-Longo, P. J. (1998) *J. Cell Biol.* **141,** 241–253
51. Tomasini-Johansson, B. R., Annis, D. S., and Mosher, D. F. (2006) *Matrix Biol.* **25,** 282–293
52. Xu, J., Maurer, L. M., Hoffmann, B. R., Annis, D. S., and Mosher, D. F. (2010) *J. Biol. Chem.* **285,** 8563–8571
53. Schwarz-Linek, U., Werner, J. M., Pickford, A. R., Gurusiddappa, S., Kim, J. H., Pilka, E. S., Briggs, J. A., Gough, T. S., Höök, M., Campbell, I. D., and Potts, J. R. (2003) *Nature* **423,** 177–181
54. Bingham, R. J., Rudiño-Piñera, E., Meenan, N. A., Schwarz-Linek, U., Turkenburg, J. P., Höök, M., Garman, E. F., and Potts, J. R. (2008) *Proc. Natl. Acad. Sci. U.S.A.* **105,** 12254–12258
55. Erat, M. C., Slatter, D. A., Lowe, E. D., Millard, C. J., Farndale, R. W., Campbell, I. D., and Vakonakis, I. (2009) *Proc. Natl. Acad. Sci. U.S.A.* **106,** 4195–4200
56. Marjenberg, Z. R., Ellis, I. R., Hagan, R. M., Prabhakaran, S., Höök, M., Talay, S. R., Potts, J. R., Staunton, D., and Schwarz-Linek, U. (2011) *J. Biol. Chem.* **286,** 1884–1894
57. Pickford, A. R., Smith, S. P., Staunton, D., Boyd, J., and Campbell, I. D. (2001) *EMBO J.* **20,** 1519–1529